nanomaterials

MDPI

Article

Unexpected Phonon Behaviour in $BiFe_xCr_{1-x}O_3$, a Material System Different from Its $BiFeO_3$ and $BiCrO_3$ Parents

Cameliu Himcinschi [1,*], Felix Drechsler [1], David Sebastian Walch [2,3], Akash Bhatnagar [2,3], Alexei A. Belik [4] and Jens Kortus [1]

[1] Institute of Theoretical Physics, TU Bergakademie Freiberg, D-09596 Freiberg, Germany; felix.drechsler@student.tu-freiberg.de (F.D.); jens.kortus@physik.tu-freiberg.de (J.K.)
[2] Zentrum für Innovationskompetenz SiLi-nano, Martin-Luther-Universität Halle-Wittenberg, D-06120 Halle (Saale), Germany; david.knoche@physik.uni-halle.de (D.S.W.); akash.bhatnagar@physik.uni-halle.de (A.B.)
[3] Institut für Physik, Martin-Luther-Universität Halle-Wittenberg, D-06120 Halle (Saale), Germany
[4] International Center for Materials Nanoarchitectonics (WPI-MANA), National Institute for Materials Science (NIMS), Namiki 1-1, Ibaraki, Tsukuba 305-0044, Japan; alexei.belik@nims.go.jp
* Correspondence: himcinsc@physik.tu-freiberg.de

Abstract: The dielectric function and the bandgap of $BiFe_{0.5}Cr_{0.5}O_3$ thin films were determined from spectroscopic ellipsometry and compared with that of the parent compounds $BiFeO_3$ and $BiCrO_3$. The bandgap value of $BiFe_{0.5}Cr_{0.5}O_3$ is lower than that of $BiFeO_3$ and $BiCrO_3$, due to an optical transition at ~2.27 eV attributed to a charge transfer excitation between the Cr and Fe ions. This optical transition enables new phonon modes which have been investigated using Raman spectroscopy by employing multi-wavelengths excitation. The appearance of a new Raman mode at ~670 cm^{-1} with a strong intensity dependence on the excitation line and its higher order scattering activation was found for both $BiFe_{0.5}Cr_{0.5}O_3$ thin films and $BiFe_xCr_{1-x}O_3$ polycrystalline bulk samples. Furthermore, Raman spectroscopy was also used to investigate temperature induced structural phase transitions in $BiFe_{0.3}Cr_{0.7}O_3$.

Keywords: Raman spectroscopy; thin films; spectroscopic ellipsometry; charge transfer; phase transition; multiferroics; $BiFe_xCr_{1-x}O_3$

Citation: Himcinschi, C.; Drechsler, F.; Walch, D.S.; Bhatnagar, A.; Belik, A.A.; Kortus, J. Unexpected Phonon Behaviour in $BiFe_xCr_{1-x}O_3$, a Material System Different from Its $BiFeO_3$ and $BiCrO_3$ Parents. *Nanomaterials* **2022**, *12*, 1607. https://doi.org/10.3390/nano12091607

Academic Editor: Sam Lofland

Received: 31 March 2022
Accepted: 5 May 2022
Published: 9 May 2022

1. Introduction

Bi_2FeCrO_6 was first theoretically proposed as a bismuth-based multiferroic material having large spontaneous magnetisation and polarisation by means of first principle studies by Baettig et al. [1,2]. Following this theoretical prediction, Bi_2FeCrO_6 epitaxial films have also been synthesised and its multiferroic character demonstrated [3,4]. Consequently, a lot of attention was dedicated to the characterisation of structural, ferroelectric and multiferroic properties of the material, and to the optimisation of the growth parameters for thin films [5–8]. Promising photovoltaic properties, the low bandgap and the possibility to tune it by the growth conditions, cationic ordering, and the domain size have attracted a lot of attention in recent years [9–13]. Various heterostructures or $BiCrO_3/BiFeO_3$ superlattices with different thicknesses and repetitions have been proposed for designing efficient ferroelectric photovoltaic devices [14–16].

Raman spectroscopy is an established method to detect subtle structural changes induced by strain or temperature and it has been already very successfully applied to the study of the lattice dynamics in the class of oxides with perovskite structures. However, in the case of Bi_2FeCrO_6 there are very few Raman or infrared spectroscopic studies reported [17–19].

In the present paper Raman spectroscopy was used in combination with spectroscopic ellipsometry for the characterisation of $BiFe_{0.5}Cr_{0.5}O_3$ thin films and polycrystalline

$BiFe_xCr_{1-x}O_3$ materials. It was thus possible to provide the evidence of light induced phonon modes and to follow the temperature induced phase transitions by Raman spectroscopy in these material systems. It should be mentioned that Bi_2FeCrO_6 is commonly used in literature for double perovskite structure with alternating Fe and Cr in the unit cell [14]. $BiFe_{0.5}Cr_{0.5}O_3$, although an equivalent representation of the same stoichiometry, allows for some deviation from the ideal 1:1 ordering expected from a typical Bi_2FeCrO_6 unit cell. In this paper, for the sake of simplicity and consistency, $BiFe_{0.5}Cr_{0.5}O_3$ (BFCO) is used for the stoichiometry of the films which also allows us to address other investigated stoichiometries for $BiFe_xCr_{1-x}O_3$ bulk samples.

2. Materials and Methods

Epitaxial $BiFe_{0.5}Cr_{0.5}O_3$ films with thickness of 120–200 nm were grown on $SrTiO_3$ $(001)_c$ substrates using pulsed laser deposition (SURFACE systems + technology PLD-Workstation (Hueckelhoven, Germany), Coherent KrF excimer laser (Santa Clara, CA, USA)). A stoichiometric ceramic $BiFe_{0.5}Cr_{0.5}O_3$ target was placed 60 mm below the substrate. During the deposition the substrate was kept at a temperature of 700 °C and exposed to 0.01 mbar oxygen partial pressure inside the chamber. The laser pulses were set to a pulse energy of 136 mJ with a repetition rate of 2 Hz. After finishing the deposition, the film was cooled at a high oxygen partial pressure (>200 mbar) with a rate of 5 °C/min. The crystallinity and phase purity of the BFCO films were confirmed by X-ray analysis (see Figure S1 in Supplementary Materials). $BiFe_xCr_{1-x}O_3$ (x = 0.3, 0.4, 0.6, 0.7) bulk polycrystalline samples were prepared from stoichiometric mixtures of Bi_2O_3 (99.9999%), Fe_2O_3 (99.999%), and Cr_2O_3 (99.9%) (Rare Metallic Co. Ltd., Tokyo, Japan) at high-pressure, high-temperature conditions of about 6 GPa. The sample with x = 0.7 was annealed at about 1550 K in an Au capsule for 90 min. The samples with x = 0.3, 0.4, 0.6 were annealed at about 1700 K in Pt capsules for 60 min. After annealing, quenching was performed by turning off heating current, and then pressure was slowly released.

The ellipsometric measurements were performed at room temperature at four angles of incidence (55°, 60°, 65° and 70°) using a M2000 ellipsometer from J.A. Woollam Company (Lincoln, NE, USA).

The micro-Raman measurements were performed with a LabRam Horiba Jobin Yvon spectrometer (Villeneuve d'Ascq, France) using 325, 442, 532, and 633 nm laser lines for excitation. A 50× magnification objective (N.A. 0.55) was used to focus and collect the scattered light, while the laser power was set low enough (below 1.5 mW for all lasers) in order to avoid damage of the samples surface and any influence of laser induced heating on the Raman spectra. All spectra were recorded in backscattering geometry. Temperature-dependent Raman measurements from 90 K up to 700 K were carried out using a LinkamTHMS-600 cooling stage (Salfords Redhill, UK) and a Linkam TS 1200 heating chamber (Salfords Redhill, UK) placed under the Raman microscope.

3. Results and Discussions

3.1. Ellipsometry Dielectric Function

First, a bare $SrTiO_3$ substrate was measured using ellipsometry, its optical response being modelled using a sum of Gaussian oscillators which ensures the Kramer–Kronig consistency of the real and imaginary parts of dielectric function. The determined dielectric function of the $SrTiO_3$ substrate was further used for the evaluation of the film/substrate system. In a second step, the absorption free energy range (below 1.75 eV) was used in order to estimate the thickness of the BFCO films using a four-layer model (substrate/film/roughness layer/ambient). The procedure used here was also applied previously for the determination of the optical constants of $BiFeO_3$ films [20]. The equations relating the ellipsometric parameters to the dielectric function can be found in [21]. The optical response of the film was modelled by a Cauchy dispersion relation ($n = A_n + B_n/\lambda^2$) (describing the refractive index in this spectral range. In a third step, using the thickness and the roughness obtained in the second step as an initial guess, the ellipsometric data were evaluated in the energy

range up to 6 eV describing the line shape of the imaginary part of the dielectric function of the film as a sum of Gaussian oscillators, while its real part is generated according to the Kramers–Kronig relation.

Using the method mentioned above a thinner (~120 nm) and a thicker (~200 nm) film with an optical roughness of ~4 nm, were evaluated using a multi-sample analysis method in order to avoid correlations between the fit parameters of the dielectric function and the thickness. Evaluating the films separately delivered nearly the same results, with an error in the determination of the thickness and roughness of ± 1 nm, which indicate that both films have the same optical properties. The thickness values obtained from ellipsometry were in good agreement with the expected nominal thickness from the PLD growth.

The determined dielectric function of the BFCO is plotted in Figure 1 as a function of energy. The energy position of the Gaussian oscillators obtained from the fit at 2.27, 3.69, and 5.25 eV are marked in the same figure by arrows. It should be mentioned that also a 4th peak located at 9.6 eV, i.e., outside the measured range, had to be considered. In the same figure the energy position of the laser lines used as excitation for the Raman spectroscopy measurements are also indicated by dotted vertical lines.

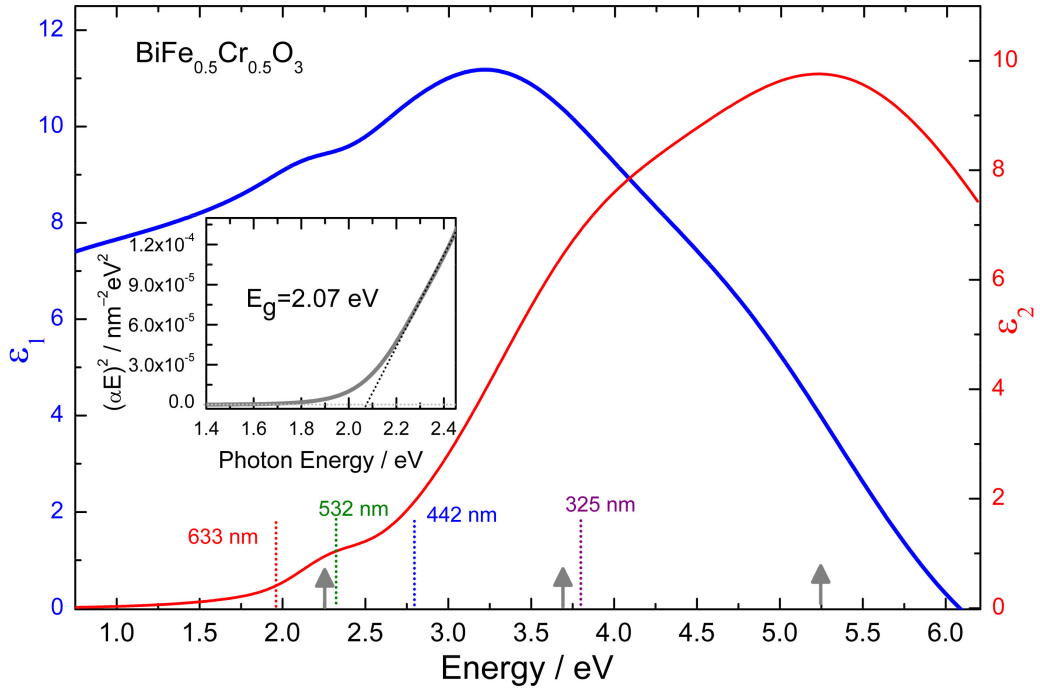

Figure 1. Real (ε_1) and imaginary (ε_2) part of $BiFe_{0.5}Cr_{0.5}O_3$ dielectric function. The dotted vertical lines indicate the energy position of the laser lines used for Raman spectroscopy, while the vertical grey arrows show the energy position of the absorption peaks. The inset show the linear extrapolation of $(\alpha E)^2$ to zero absorption which give the value of the optical band gap.

From the real ε_1 and imaginary ε_2 part of the dielectric function, the complex refractive index $n + ik$ is calculated. The absorption coefficient α can be derived from the extinction coefficient k as: $\alpha = 4\pi k/\lambda$. The absorption coefficient of BFCO is plotted in Figure 2 in comparison to the absorption coefficient of $BiFeO_3$ and $BiCrO_3$ films. It is very clear from the figure (especially from the zoom in the inset of Figure 2) that the BFCO films start to absorb at lower energies than its parent materials $BiFeO_3$ and $BiCrO_3$. The arrow at 2.27 eV indicates the position of the first absorption peak as determined from ellipsometry. These results corroborate that BFCO is promising material in the field of photovoltaic applications due to its extended absorption of the solar spectrum when compared with $BiFeO_3$ or $BiCrO_3$.

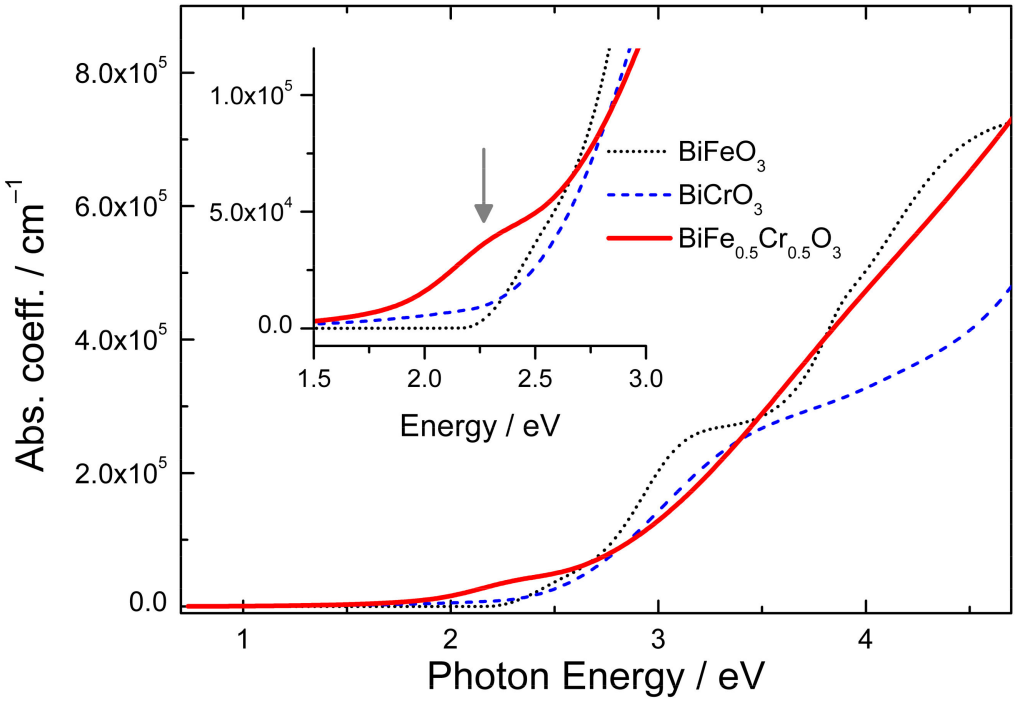

Figure 2. Absorption coefficient of $BiFe_{0.5}Cr_{0.5}O_3$ in comparison with the absorption coefficients of $BiFeO_3$ and $BiCrO_3$. The inset show a zoom of the absorption onset region with the vertical arrow indicating the first absorption peak at ~2.27 eV.

In order to gain a better look on the onset of the absorption, this region was analysed in detail. The optical gap of the BFCO films was determined by using the procedure for bandgap determination proposed by Tauc et al. [22] that was already successfully applied to $BiFeO_3$ and $BiCrO_3$ films [23–25].

Using the proportionality $(\alpha E)^2 \sim E - E_g$ and extrapolating to zero absorption, a value of the energy gap E_g of 2.07 eV was obtained, as can be seen in the inset of Figure 1. This value is well below the values of the direct optical gaps of 2.8 eV or 2.95 eV reported for $BiFeO_3$ [23,24] and $BiCrO_3$ [25], respectively. The bandgap value obtained is, however, in good agreement with the values determined for Bi_2FeCrO_6 films which were found to be strongly influenced by the deposition conditions, cation ordering, domain size, or film thickness [9,10,12,13,26–28].

Considering the first peak determined in the imaginary part of the dielectric function, ε_2, of BFCO at ~2.27 eV, its position is very close to the first absorption peaks observed in stoichiometrically similar Bi_2FeCrO_6 films [11] or in $LaFe_{0.5}Cr_{0.5}O_3$ [29,30]. Its origin was attributed to a charge transfer excitation between Cr and Fe, being only present in the Fe/Cr mixed systems [11,29–31]. The lowest transition in Bi_2FeCrO_6 was also predicted to be between the Fe3d and Cr3d states using ab initio calculations in the pioneering work of Baettig et al. [1]. The appearance of this charge transfer band plays a crucial role in understanding the Raman spectra of BFCO that will be presented in the next section.

3.2. Raman Spectroscopy

The structure of $BiFe_{0.5}Cr_{0.5}O_3$ is composed of alternating ABO_3-$AB'O_3$ perovskite cells (also called as double-perovskite structure $A_2BB'O_6$). Structural studies using XRD and neutron diffraction showed that at room temperature $BiFe_{0.5}Cr_{0.5}O_3$ has a trigonal lattice of the space group *R3c* (No. 161) very similar to that of the $BiFeO_3$ [32,33]. In the case of $BiFeO_3$, for this space group, group theory predicts $4A_1$ and 9E polar Raman modes [34–36]. The Raman spectrum of a 200 nm thick $BiFe_{0.5}Cr_{0.5}O_3$ film deposited on the $SrTiO_3$ substrate measured with an excitation of 633 nm is shown by the continuous line in the upper part of Figure 3. The Raman signal is dominated by the broad peaks of the

substrate. In order to extract the $BiFe_{0.5}Cr_{0.5}O_3$ signal, the substrate spectrum (dotted line in Figure 3) was measured by focusing the laser at a depth of about 30 μm below the film surface, and subsequently subtracted from the film/substrate spectrum. The difference spectrum is shown by the red line in the upper part of Figure 3. As can be seen, besides some weak peaks below 600 cm^{-1}, there is a prominent peak at 670 cm^{-1}. This peak was attributed in a previous Raman study of $BiFe_{0.5}Cr_{0.5}O_3$ films to the $SrTiO_3$ substrate due to its proximity to the substrate peak [18]. As can be seen in the lower panel of Figure 3, the 670 cm^{-1} peak is also present in the difference spectrum obtained with the 532 nm and nearly absent in the case of 442 nm excitation line, using the same procedure of subtraction for these excitations. Such a strong intensity dependence on the excitation wavelength is a clear indication of coupling phenomena.

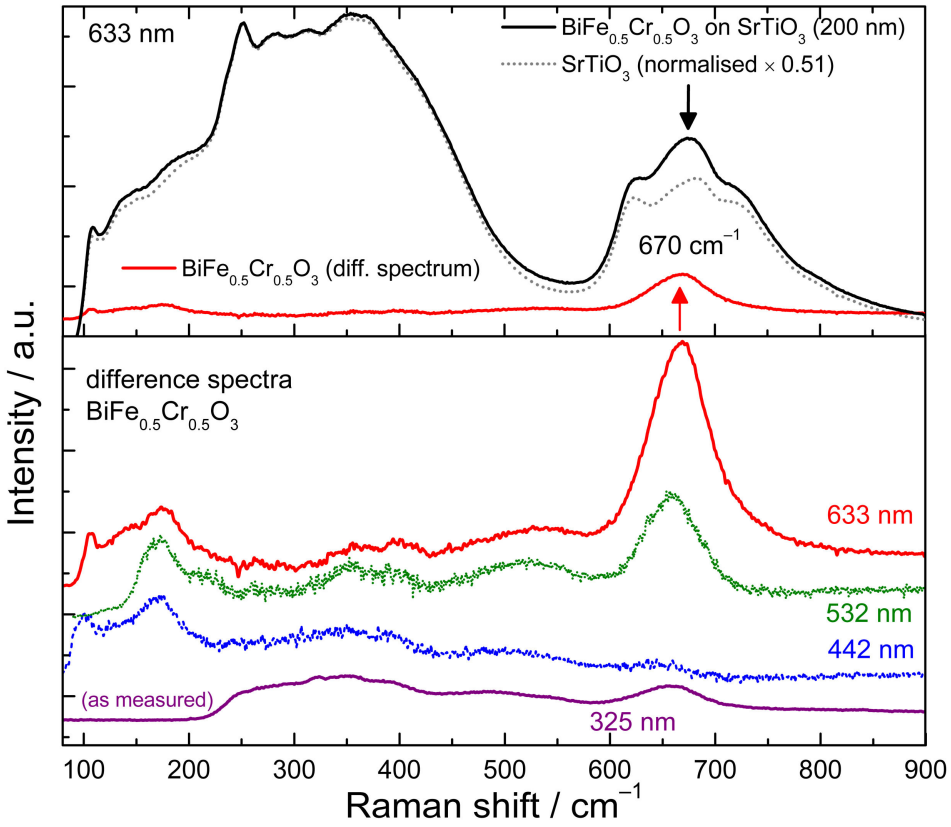

Figure 3. Raman spectra of a 200 nm $BiFe_{0.5}Cr_{0.5}O_3$ thin film on $SrTiO_3$ substrate and of the substrate normalised at the same intensity in the 200–400 cm^{-1} region, measured with an excitation of 633 nm. The corresponding film signal was calculated as a difference spectrum of the two (upper panel). The difference spectra of the thin film obtained with different excitations lines (633 nm, 532 nm, and 442 nm) and the as measured spectrum with the 325 nm excitation (lower panel).

Its origin will be discussed in the following part using also the ellipsometry data. The penetration depth d of light in a material can be calculated from the absorption coefficient α or from the extinction coefficient k as: $d = 1/\alpha = \lambda/4\pi k$. Considering the determined absorption coefficient (Figure 2) the penetration depths of the 633, 532, and 442 nm light are 750, 248, and 115 nm, respectively. This of course means that the laser light penetrates through the film and that also a substrate signal is expected when measuring 100–200 nm thick films. On the other hand, when measuring the Raman spectra using 325 nm excitation, which has a penetration depth of only 25 nm in $BiFe_{0.5}Cr_{0.5}O_3$ the measured spectra correspond only to the film. As can be seen in Figure 3, the peak at 670 cm^{-1} is also present in the spectra recorded with the 325 nm excitation. This clearly indicates that the 670 cm^{-1} peak is intrinsic to $BiFe_{0.5}Cr_{0.5}O_3$ and not to the substrate. Its strong intensity dependence

on the excitation energy can be understood by the proximity of the energy of the excitation laser to the absorption peaks (see Figure 1). The 633 nm and 532 nm wavelengths are close to the first absorption peak, 325 nm is close to the second absorption peak, while 442 nm is far from such resonances and the Raman peak at 670 cm^{-1} is hardly observable for this last excitation.

It should be also mentioned that the Raman spectra for Bi_2FeCrO_6 previously published in the literature [18] show a very strong peak at ~830 cm^{-1} which was also found in the case of Cr doping of $BiFeO_3$ or for $BiFe_xCr_{1-x}O_3$ powder, and was attributed to Cr-O vibration [19,37]. In our films, as it can be seen in Figure 3, we do not observe such a peak. However, such peak was found previously in different species of chromium oxides species [38–41]. The presence of this peak in the studies [18,19] may indicate that, in those cases, $BiFe_xCr_{1-x}O_3$ were not a pure phase and maybe contained species of chromium oxides.

In order to shed light on the origin of the 670 cm^{-1} peak, we measured Raman spectra of bulk $BiFe_xCr_{1-x}O_3$ (x = 0.3, 0.4, 0.6, 0.7) polycrystalline samples. The spectra measured with 633 nm excitation are shown in Figure 4 together with the difference spectra of the 200 nm $BiFe_{0.5}Cr_{0.5}O_3$ film, and of the parent compounds $BiFeO_3$ and $BiCrO_3$. As can be seen, a peak at 660–670 cm^{-1} is present in all the spectra of Fe-Cr containing systems and absent for $BiFeO_3$ and $BiCrO_3$. On the other hand, no peak is measured between 800 and 900 cm^{-1}, which indicates the absence of secondary chromium oxides phases in our thin films and bulk samples.

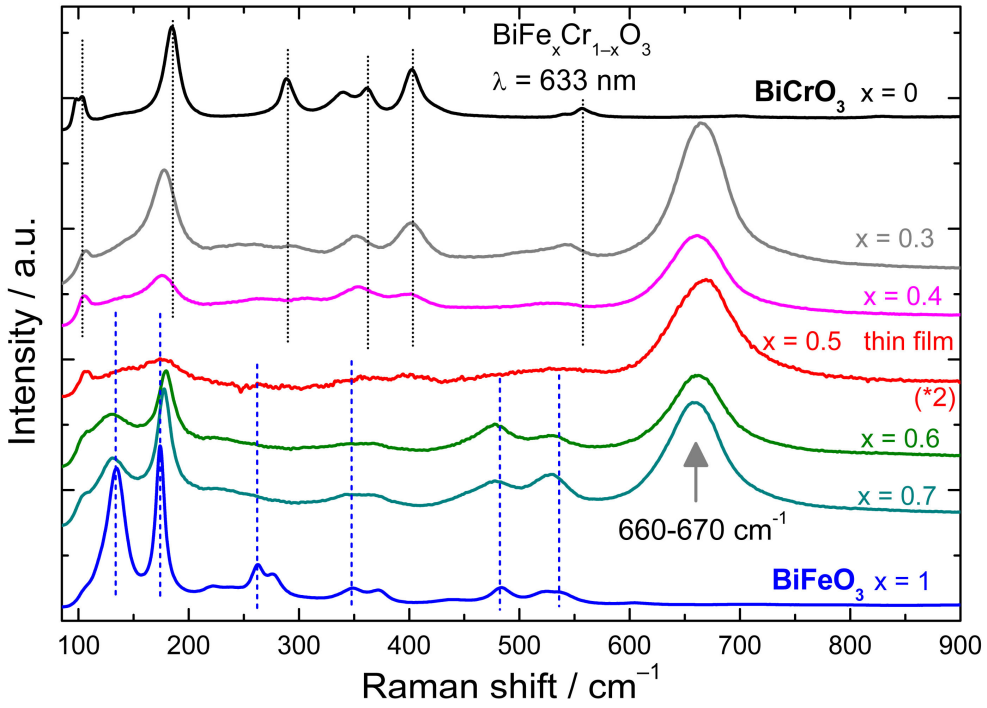

Figure 4. The difference spectrum of the $BiFe_{0.5}Cr_{0.5}O_3$ thin film compared to the spectra of bulk $BiFe_xCr_{1-x}O_3$, and of the parent compounds $BiCrO_3$ and $BiFeO_3$ measured with 633 nm excitation. Note the strong peak at 660–670 cm^{-1} which is detected only for the samples with a Fe/Cr mixture.

For x = 0.7, 0.6, and 0.5 the Raman spectra are resembling more to those of $BiFeO_3$, indicating the expected *R3c* space group. On the other hand, for x = 0.3 and 0.4 the spectra are more $BiCrO_3$-like (*C2/c* space group) [25]. The relative intensity of the 660–670 cm^{-1} mode in respect to the polar mode (A_{1LO}-E_{LO}) at 172 cm^{-1} ($BiFeO_3$-like) [36] or to the A_g mode at 185 cm^{-1} ($BiCrO_3$-like) [42] is strongest for the highest Fe-Cr mixture (x = 0.4, 0.5, and 0.6). This fact corroborated to the absence of the peak in the case of $BiFeO_3$ and $BiCrO_3$ indicate that the origin of the peak is related to the simultaneous presence of Fe and Cr in the structure. A very similar peak, at similar positions, has been measured also

for other perovskite systems with Fe/Cr intermixing. For example, for $HoFe_{1-x}Cr_xO_3$ a peak at 670 cm^{-1} was attributed to oxygen breathing mode (A_g-like) and was found to be activated due to the charge transfer between Fe^{3+} and Cr^{3+} ions (mediated by O^{2-}) playing a role in electron–phonon coupling [31]. As for our system, the mode was absent or having a very low intensity for the stoichiometry with only Fe or only Cr. Fe-Cr charge transfer effects activated a similar oxygen vibration mode related to the octahedron breathing in the case of $LaFe_{0.5}Cr_{0.5}O_3$ [30] or $LaFe_xCr_{1-x}O_3$ systems [29,43] where the mode again vanished in the case of the parent compounds. All these aspects also indicate that in the case of $BiFe_xCr_{1-x}O_3$ the 670 cm^{-1} mode is an oxygen-related mode activated by the charge transfer between the Fe and Cr ion, mediated by the excitation light and is strongest when the energy of the incident photons is close to the first absorption peak at 2.27 eV (corresponding to charge transfer excitation between Cr and Fe). This was observed in case of our $BiFe_{0.5}Cr_{0.5}O_3$ films, where the intensity of the 670 cm^{-1} peak was higher for 633 nm and 532 nm than for 442 nm excitation. Raman spectra for the $BiFe_{0.3}Cr_{0.7}O_3$ polycrystalline sample measured with the same excitation lines are shown in Figure 5. Additionally, in this case the strongest peak at 667 cm^{-1} is measured when exciting with 633 nm and 532 nm. Moreover, the second order of this peak at 1325 cm^{-1} and even the third order at ~1995 cm^{-1} are observable for these two excitations (the third order peak for 532 nm is not shown due to the coincidence with some CCD artefacts), while for 442 nm even the first order is very low in intensity. A very similar behaviour was also observed for the other stoichiometries of the polycrystalline $BiFe_xCr_{1-x}O_3$ samples.

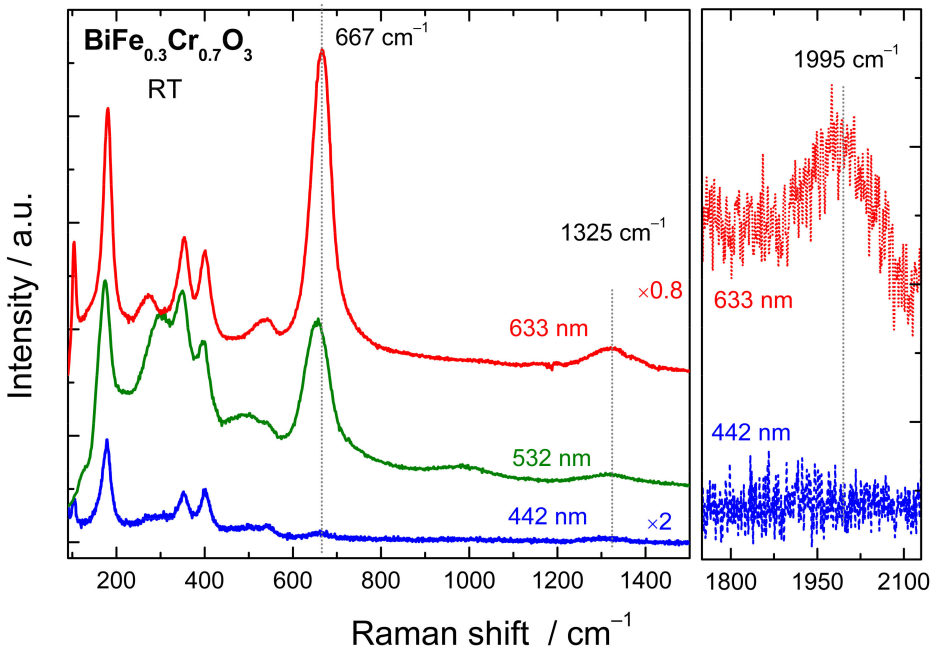

Figure 5. Comparison of the Raman spectra of bulk $BiFe_{0.3}Cr_{0.7}O_3$ recorded with different excitation lines in the range of the first, second, and third order of the mode at ~667 cm^{-1}.

The multiple-order Raman scattering and the resonance effects were explained in the frame of the Franck–Condon type mechanism for rare-earth manganite systems [44–46]. The same Franck–Condon picture was also used to explain the Fe-Cr charge transfer which resonantly activates the oxygen breathing mode and its higher-orders. [31,43].

The temperature dependent Raman spectra of $BiFe_{0.3}Cr_{0.7}O_3$ polycrystalline sample in the 90–700 K temperature range are shown in Figure 6. With increasing the temperature up to 450 K the Raman peaks below 600 cm^{-1} are decreasing in intensity, shifting to lower wavenumbers and become broader, which is a characteristic thermal behaviour related to anharmonicity of the phonon vibrations. However, the position and the broadening of the mode at 670 cm^{-1} are much less affected by the temperature. This fact could be

another indication that the activation of the mode is related to the Fe-Cr charge transfer. Starting with 475 K some new peaks are developing as indicated by the arrows in Figure 6, while peaks corresponding to the lower temperatures (vertical lines) are disappearing. Such a behaviour points to a structural phase transition. The new peaks which develop above 475 K are also present in the spectra measured at 700 K. After subsequent cooling at room temperature the same spectrum as before heating is obtained, indicating that the phase transition is reversible. In the case of $BiCrO_3$, Raman spectroscopy revealed a reversible phase transition from *C2/c* monoclinic phase to a *pnma* orthorhombic phase above 400 K [25]. For $BiFe_{0.3}Cr_{0.7}O_3$ the transition temperature increases. Syncrotron X-ray powder diffraction (SXRD) data indicates a *pbam* symmetry ($PbZrO_3$-type) at room temperature while at 600 K the structure changes to *pnma* symmetry of $GdFeO_3$-type (see Figure S2 in Supplementary Materials). The refined lattice parameters obtained from the Rietveld analysis method of the SXRD data by means of *RIETAN-2000* program [47], indicate that the phase transition is accompanied by a reduction in the volume of the unit cell by a factor of two.

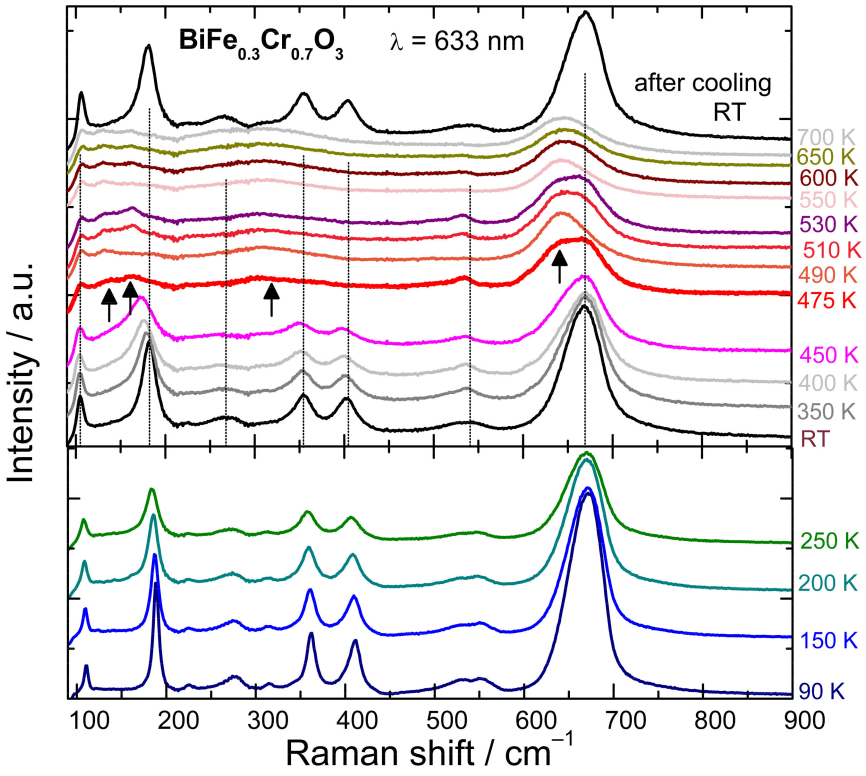

Figure 6. Temperature dependence (90–700 K) of the Raman spectra for bulk $BiFe_{0.3}Cr_{0.7}O_3$ showing a reversible phase transition above 475 K.

4. Conclusions

In conclusion, in $BiFe_{0.5}Cr_{0.5}O_3$ thin films and $BiFe_xCr_{1-x}O_3$ bulk appearance of a new Raman mode at ~670 cm^{-1} which is absent in the $BiFeO_3$ and $BiCrO_3$ parent compounds was evidenced by Raman spectroscopy. The mode was attributed to an oxygen (octahedral) breathing vibration which is mediated by the charge transfer between the Fe and Cr ions. This charge transfer corresponds to an optical absorption peak at ~2.27 eV for $BiFe_{0.5}Cr_{0.5}O_3$ which lowers the bandgap of the material compared to the parent compound as was found by spectroscopic ellipsometry. On the other hand, Franck–Condon mechanism is manifested by a strong dependence of the intensity of the 670 cm^{-1} Raman peak on the excitation wavelength, and resonant activation of its higher scattering orders. For $BiFe_{0.3}Cr_{0.7}O_3$ Raman spectroscopy revealed a reversible temperature induce structural phase transition.

Supplementary Materials: The following supporting information can be downloaded at: https://www.mdpi.com/article/10.3390/nano12091607/s1, Figure S1: X-Ray diffraction 2θ-ω scan comprising (001) and (002) peaks of STO substrate and 200 nm BFCO thin film (left panel). Topography scan (5 × 5 μm2) acquired by atomic force microscopy (contact mode) of the same BFCO thin film (right panel); Figure S2: High-temperature synchrotron powder X-ray diffraction measurements of the BiFe0.3Cr0.7O3 sample confirmed the existence of a reversible high-temperature structural phase transition from the PbZrO3-type structure (at room temperature) to the GdFeO3-type structure (at 600 K) [47,48].

Author Contributions: C.H. proposed the study, performed, and analysed the ellipsometric measurements and part of the Raman measurements and wrote the manuscript with contributions from all other authors; F.D. performed and analysed the Raman measurements; A.B. and D.S.W. grown the thin films; A.A.B. prepared the polycrystalline samples and performed and analysed the X-Ray diffraction. measurements; J.K. reviewed the manuscript with ideas on data interpretation. All authors have read and agreed to the published version of the manuscript.

Funding: Open Access Funding by the Publication Fund of the TU Bergakademie Freiberg. This research was funded by German Research Foundation (DFG), Project No. 441856638 and Project No. 31047526, and by Bundesministerium für Bildung und Forschung (BMBF) Project No. 03Z22HN12.

Institutional Review Board Statement: Not applicable.

Informed Consent Statement: Not applicable.

Data Availability Statement: The data presented in this study are available on request from the corresponding author.

Acknowledgments: Open Access Funding by the Publication Fund of the TU Bergakademie Freiberg. CH acknowledges the German Research Foundation (DFG), Project No. 441856638 for financial support. A.B. and D.W. acknowledge the financial support from Bundesministerium für Bildung und Forschung (BMBF) Project No. 03Z22HN12, Deutsche Forschungsgemeinschaft (DFG) within Sonderforschungsbereiche (SFB) 762 (project A12), and Europäischen Fonds für regionale Entwicklung (EFRE) Sachsen-Anhalt. The synchrotron radiation experiments were performed at SPring-8 [48] with the approval of Japan Synchrotron Radiation Research Institute (Proposal No. 2021A1334). We thank Kobayashi, S. for his assistance at BL02B2 of SPring-8.

Conflicts of Interest: The authors declare no conflict of interest.

References

1. Baettig, P.; Spaldin, N.A. Ab initio prediction of a multiferroic with large polarization and magnetization. *Appl. Phys. Lett.* **2005**, *86*, 012505. [CrossRef]
2. Baettig, P.; Ederer, C.; Spaldin, N.A. First principles study of the multiferroics $BiFeO_3$, Bi_2FeCrO_6, and $BiCrO_3$: Structure, polarization, and magnetic ordering temperature. *Phys. Rev. B* **2005**, *72*, 214105. [CrossRef]
3. Nechache, R.; Harnagea, C.; Pignolet, A.; Normandin, F.; Veres, T.; Carignan, L.P.; Ménard, D. Growth, structure, and properties of epitaxial thin films of first-principles predicted multiferroic Bi_2FeCrO_6. *Appl. Phys. Lett.* **2006**, *89*, 102902. [CrossRef]
4. Nechache, R.; Harnagea, C.; Pignolet, A.; Carignan, L.P.; Ménard, D. Epitaxial Bi2FeCrO6 multiferroic thin films. *Philos. Mag. Lett.* **2007**, *87*, 231–240. [CrossRef]
5. Nechache, R.; Harnagea, C.; Carignan, L.-P.; Gautreau, O.; Pintilie, L.; Singh, M.P.; Ménard, D.; Fournier, P.; Alexe, M.; Pignolet, A. Epitaxial thin films of the multiferroic double perovskite Bi_2FeCrO_6 grown on (100)-oriented $SrTiO_3$ substrates: Growth, characterization, and optimization. *J. Appl. Phys.* **2009**, *105*, 061621. [CrossRef]
6. Nechache, R.; Rosei, F. Recent progress in nanostructured multiferroic Bi_2FeCrO_6 thin films. *J. Solid State Chem.* **2012**, *189*, 13–20. [CrossRef]
7. Sha, L.; Miao, J.; Wu, S.Z.; Xu, X.G.; Jiang, Y.; Qiao, L.J. Double-perovskite multiferroic Bi_2FeCrO_6 polycrystalline thin film: The structural, multiferroic, and ferroelectric domain properties. *J. Alloys Compd.* **2013**, *554*, 299–303. [CrossRef]
8. Wu, H.; Pei, Z.; Xia, W.; Lu, Y.; Leng, K.; Zhu, X. Structural, magnetic, dielectric and optical properties of double-perovskite Bi_2FeCrO_6 ceramics synthesized under high pressure. *J. Alloys Compd.* **2020**, *819*, 153007. [CrossRef]
9. Nechache, R.; Harnagea, C.; Li, S.; Cardenas, L.; Huang, W.; Chakrabartty, J.; Rosei, F. Bandgap tuning of multiferroic oxide solar cells. *Nat. Photonics* **2015**, *9*, 61–67. [CrossRef]
10. Li, S.; AlOtaibi, B.; Huang, W.; Mi, Z.; Serpone, N.; Nechache, R.; Rosei, F. Epitaxial Bi_2FeCrO_6 Multiferroic Thin Film as a New Visible Light Absorbing Photocathode Material. *Small* **2015**, *32*, 4018–4026. [CrossRef]

11. Nechache, R.; Huang, W.; Li, S.; Rosei, F. Photovoltaic properties of Bi_2FeCrO_6 films epitaxially grown on (100)-oriented silicon substrates. *Nanoscale* **2016**, *8*, 3237–3243. [CrossRef]
12. Quattropani, A.; Stoeffler, D.; Fix, T.; Schmerber, G.; Lenertz, M.; Versini, G.; Rehspringer, J.L.; Slaoui, A.; Dinia, A.; Colis, S. Band-Gap Tuning in Ferroelectric Bi_2FeCrO_6 Double Perovskite Thin Films. *J. Phys. Chem. C* **2017**, *122*, 1070–1077. [CrossRef]
13. Quattropani, A.; Makhort, A.S.; Rastei, M.V.; Versini, G.; Schmerber, G.; Barre, S.; Dinia, A.; Slaoui, A.; Rehspringer, J.-L.; Fix, T.; et al. Tuning photovoltaic response in Bi_2FeCrO_6 films by ferroelectric poling. *Nanoscale* **2018**, *10*, 13761–13766. [CrossRef]
14. Tablero, C. Photovoltaic application of the multiferroic Bi_2FeCrO_6 double perovskite. *Sol. Energy* **2016**, *137*, 173–178. [CrossRef]
15. Guo, K.; Wang, X.; Zhang, R.; Fu, Z.; Zhang, L.; Ma, G.; Deng, C. Multiferroic oxide BFCNT/BFCO heterojunction black silicon photovoltaic devices. *Light Sci. Appl.* **2021**, *10*, 201. [CrossRef]
16. Zhang, S.; Xiao, H.Y.; Peng, S.M.; Yang, G.X.; Liu, Z.J.; Zu, X.T.; Li, S.; Singh, D.J.; Martin, L.W.; Qiao, L. Band-Gap Reduction in $(BiCrO_3)m/(BiFeO_3)n$ Superlattices: Designing Low-Band-Gap Ferroelectrics. *Phys. Rev. Appl.* **2018**, *10*, 044004. [CrossRef]
17. Kamba, S.; Nuzhnyy, D.; Nechache, R.; Závěta, K.; Nižňanský, D.; Šantavá, E.; Harnagea, C.; Pignolet, A. Infrared and magnetic characterization of multiferroic Bi_2FeCrO_6 thin films over a broad temperature range. *Phys. Rev. B* **2008**, *77*, 104111. [CrossRef]
18. Meng, D.; Kang, T.; Bi, L.; Zhang, H.; Zhai, J.; Bai, F. Temperature-driven structural phase transition in double perovskite Bi_2FeCrO_6 films. *Appl. Phys. Express* **2020**, *13*, 011008. [CrossRef]
19. Kolhatkar, G.; Ambriz-Vargas, F.; Thomas, R.; Ruediger, A. Microwave-Assisted Hydrothermal Synthesis of $BiFe_xCr_{1-x}O_3$ Ferroelectric Thin Films. *Cryst. Growth Des.* **2017**, *17*, 5697–5703. [CrossRef]
20. Himcinschi, C.; Vrejoiu, I.; Friedrich, M.; Ding, L.; Cobet, C.; Esser, N.; Alexe, M.; Zahn, D.R.T. Optical characterisation of $BiFeO_3$ epitaxial thin films grown by pulsed-laser deposition. *Phys. Status Solidi C* **2010**, *7*, 296–299. [CrossRef]
21. Azzam, R.M.A.; Bashara, N.M. *Ellipsometry and Polarized Light*; Elsevier: Amsterdam, The Netherlands, 1987; pp. 269–275.
22. Tauc, J.; Grigorovici, R.; Vancu, A. Optical Properties and Electronic Structure of Amorphous Germanium. *Phys. Status Solidi B* **1966**, *15*, 627–637. [CrossRef]
23. Himcinschi, C.; Bhatnagar, A.; Talkenberger, A.; Barchuk, M.; Zahn, D.R.T.; Rafaja, D.; Kortus, J.; Alexe, M. Optical properties of epitaxial BiFeO3 thin films grown on $LaAlO_3$. *Appl. Phys. Lett.* **2015**, *106*, 012908. [CrossRef]
24. Himcinschi, C.; Vrejoiu, I.; Friedrich, M.; Nikulina, E.; Ding, L.; Cobet, C.; Esser, N.; Alexe, M.; Rafaja, D.; Zahn, D.R.T. Substrate influence on the optical and structural properties of pulsed laser deposited $BiFeO_3$ epitaxial films. *J. Appl. Phys.* **2010**, *107*, 123524. [CrossRef]
25. Himcinschi, C.; Vrejoiu, I.; Weißbach, T.; Vijayanandhini, K.; Talkenberger, A.; Röder, C.; Bahmann, S.; Zahn, D.R.T.; Belik, A.A.; Rafaja, D.; et al. Raman spectra and dielectric function of $BiCrO_3$: Experimental and first-principles studies. *J. Appl. Phys.* **2011**, *110*, 073501. [CrossRef]
26. Rastei, M.V.; Gellé, F.; Schmerber, G.; Quattropani, A.; Fix, T.; Dinia, A.; Slaoui, A.; Colis, S. Thickness Dependence and Strain Effects in Ferroelectric Bi_2FeCrO_6 Thin Films. *ACS Appl. Energy Mater.* **2019**, *2*, 8550–8559. [CrossRef]
27. Huang, W.; Harnagea, C.; Benetti, D.; Chaker, M.; Rosei, F.; Nechache, R. Multiferroic Bi_2FeCrO_6 based p–i–n heterojunction photovoltaic devices. *J. Mater. Chem. A* **2017**, *5*, 10355–10364. [CrossRef]
28. Meng, D.; Xiao, Y.; He, H.; Liao, Y.; Zhang, H.; Zhai, J.; Chen, Z.; Martin, L.W.; Bai, F. Enhanced spontaneous polarization in double perovskite Bi_2FeCrO_6 films. *J. Am. Ceram. Soc.* **2019**, *102*, 5234–5242. [CrossRef]
29. Andreasson, J.; Holmlund, J.; Knee, C.S.; Käll, M.; Börjesson, L.; Naler, S.; Bäckström, J.; Rübhausen, M.; Azad, A.K.; Eriksson, S.G. Franck-Condon higher order lattice excitations in the $LaFe_{1-x}Cr_xO3$ (x=0, 0.1, 0.5, 0.9, 1.0) perovskites due to Fe-Cr charge transfer effects. *Phys. Rev. B* **2007**, *75*, 104302. [CrossRef]
30. Andreasson, J.; Holmlund, J.; Singer, S.G.; Knee, C.S.; Rauer, R.; Schulz, B.; Käll, M.; Rübhausen, M.; Eriksson, S.G.; Börjesson, L.; et al. Electron-lattice interactions in the perovskite $LaFe_{0.5}Cr_{0.5}O_3$ characterized by optical spectroscopy and LDA+U calculations. *Phys. Rev. B* **2009**, *80*, 075103. [CrossRef]
31. Kotnana, G.; Jammalamadaka, S.N. Band gap tuning and orbital mediated electron–phonon coupling in $HoFe_{1-x}Cr_xO_3$ ($0 \leq x \leq 1$). *J. Appl. Phys.* **2015**, *118*, 124101. [CrossRef]
32. Suchomel, M.R.; Thomas, C.I.; Allix, M.; Rosseinsky, M.J.; Fogg, A.F.; Thomas, M.F. High pressure bulk synthesis and characterization of the predicted multiferroic $Bi(Fe_{1/2}Cr_{1/2})O_3$. *Appl. Phys. Lett.* **2007**, *90*, 112909. [CrossRef]
33. McBride, B.R.; Lieschke, J.; Berlie, A.; Cortie, D.L.; Playford, H.Y.; Lu, T.; Narayanan, N.; Withers, R.L.; Yu, D.; Liu, Y. Study of the B-site ion behaviour in the multiferroic perovskite bismuth iron chromium oxide. *J. Appl. Phys.* **2018**, *123*, 154104. [CrossRef]
34. Haumont, R.; Kreisel, J.; Bouvier, P. Raman scattering of the model multiferroic oxide $BiFeO_3$: Effect of temperature, pressure and stress. *Phase Transit.* **2006**, *79*, 1043–1064. [CrossRef]
35. Hlinka, J.; Pokorny, J.; Karimi, S.; Reaney, I.M. Angular dispersion of oblique phonon modes in $BiFeO_3$ from micro-Raman scattering. *Phys. Rev. B* **2011**, *83*, 020101(R). [CrossRef]
36. Himcinschi, C.; Rix, J.; Röder, C.; Rudolph, M.; Yang, M.-M.; Rafaja, D.; Kortus, J.; Alexe, M. Ferroelastic domain identification in $BiFeO_3$ crystals using Raman spectroscopy. *Sci. Rep.* **2019**, *9*, 379. [CrossRef]
37. Deng, H.; Deng, H.; Yang, P.; Chu, J. Effect of Cr doping on the structure, optical and magnetic properties of multiferroic $BiFeO_3$ thin films. *J. Mater. Sci. Mater. Electron.* **2012**, *23*, 1215–1218. [CrossRef]
38. Hardcastle, F.D.; Wachs, I.E. Raman spectroscopy of chromium oxide supported on Al_2O_3, TiO_2 and SiO_2: A comparative study. *J. Mol. Catal.* **1988**, *46*, 173–186. [CrossRef]

39. Weckhuysen, B.M.; Wachs, I.E. Raman spectroscopy of supported chromium oxide catalysts. Determination of chromium-oxygen bond distances and bond orders. *J. Chem. Soc. Faraday Trans.* **1996**, *92*, 1969–1973. [CrossRef]
40. Weckhuysen, B.M.; Wachs, I.E. In Situ Raman Spectroscopy of Supported Chromium Oxide Catalysts: $^{18}O_2$-$^{16}O_2$ Isotopic Labeling Studies. *J. Phys. Chem. B* **1997**, *101*, 2793–2796. [CrossRef]
41. Monnereau, O.; Tortet, L.; Grigorescu, C.; Savastru, D.; Iordanescu, C.R.; Guinneton, F.; Notonier, R.; Tonetto, A.; Zhang, T.; Mihailescu, I.; et al. Chromium oxides mixtures in PLD films investigated by Raman spectroscopy. *J. Optoelectron. Adv. Mater.* **2010**, *12*, 1752–1758.
42. Talkenberger, A.; Himcinschi, C.; Weißbach, T.; Vijayanandhini, K.; Vrejoiu, I.; Röder, C.; Rafaja, D.; Kortus, J. Raman spectroscopic and X-ray diffraction investigations of epitaxial $BiCrO_3$ thin films. *Thin Solid Films* **2012**, *520*, 4590–4594. [CrossRef]
43. Andreasson, J.; Holmlund, J.; Rauer, R.; Käll, M.; Börjesson, L.; Knee, C.S.; Eriksson, A.K.; Eriksson, S.G.; Rübhausen, M.; Chaudhury, R.P. Electron-phonon interactions in perovskites containing Fe and Cr studied by Raman scattering using oxygen-isotope and cation substitution. *Phys. Rev. B* **2008**, *78*, 235103. [CrossRef]
44. Allen, P.B.; Perebeinos, V. Self-Trapped Exciton and Franck-Condon Spectra Predicted in $LaMnO_3$. *Phys. Rev. Lett.* **1999**, *83*, 4828–4831. [CrossRef]
45. Krüger, R.; Schulz, B.; Naler, S.; Rauer, R.; Budelmann, D.; Bäckström, J.; Kim, K.H.; Cheong, S.W.; Perebeinos, V.; Rübhausen, M. Orbital ordering in LaMnO3 Investigated by Resonance Raman Spectroscopy. *Phys. Rev. Lett.* **2004**, *92*, 097203. [CrossRef]
46. Iliev, M.N.; Hadjiev, V.G.; Litvinchuk, A.P.; Yen, F.; Wang, Y.Q.; Sun, Y.Y.; Jandl, S.; Laverdière, J.; Popov, V.N.; Gospodinov, M.M. Multiple-order Raman scattering from rare-earth manganites: Oxygen isotope and rare-earth substitution effects. *Phys. Rev. B* **2007**, *75*, 064303. [CrossRef]
47. Izumi, F.; Ikeda, T. A Rietveld-analysis program RIETAN-98 and its applications to zeolites. *Mater. Sci. Forum* **2000**, *321–324*, 198–205. [CrossRef]
48. Kawaguchi, S.; Takemoto, M.; Osaka, K.; Nishibori, E.; Moriyoshi, C.; Kubota, Y.; Kuroiwa, Y.; Sugimoto, K. High-throughput powder diffraction measurement system consisting of multiple MYTHEN detectors at beamline BL02B2 of SPring-8. *Rev. Sci. Instrum.* **2017**, *88*, 085111. [CrossRef]